Light-Controlled Propulsion of Catalytic Microengines

ARTICLE *in* ANGEWANDTE CHEMIE INTERNATIONAL EDITION · NOVEMBER 2011

Impact Factor: 11.26 · DOI: 10.1002/anie.201102096 · Source: PubMed

Microengines

DOI: 10.1002/anie.201102096

Light-Controlled Propulsion of Catalytic Microengines**

Alexander A. Solovev, Elliot J. Smith, Carlos C. Bof' Bufon, Samuel Sanchez, and Oliver G. Schmidt*

Control over the autonomous motion of artificial nano/micromachines is essential for real biomedical and nanotechnological applications. Consequently, a complete nanomachine should be able to be turned on and off at will. Developments over the last few years on synthetic catalytic nano/microengines and motors have enabled the harvesting of chemical energy from local molecules and transforming it into an effective autonomous motion.[1] Several impressive applications have recently reported the use of artificial micromachines for the detection of biomolecules with roving nanomotors,[2] transport of animal cells in a fluid,[3] and other microcargo delivery.[4–7]

Recently, the use of a light source has been implemented to propel microparticle-based motors[8] generated by a self-diffusiophoretic mechanism. Despite this interesting approach, the motion of the particles is limited by the dissolution of the materials and to the ultraviolet (UV) spectrum.[9] Moreover, a reversible method to start and stop the propulsion of micromotors by a visible-light source remains a challenge.

Here we report the tuning of the propulsion power of Ti/Cr/Pt catalytic microengines (μ-engines) through illumination of a solution by a white-light source. We show that light suppresses the generation of microbubbles, stopping the engines if they are fixed-to or self-propelled above a platinum-patterned surface. The μ-engines are reactivated by dimming the light source that illuminates the fuel solution. The illumination of the solution with visible light in the presence of Pt diminishes the concentration of hydrogen peroxide fuel and degrades the surfactant, consequently reducing the motility of the microjets. Electrochemical measurements and analysis of the surface tension support our findings. We also study the influence of different wavelengths over the visible spectrum (500–750 nm) on the formation of microbubbles.

Rolled-up Ti/Cr/Pt catalytic μ-engines with diameters of 5–10 μm and a length of 50 μm were prepared as described previously elsewhere[10–12] and in the Experimental Section. Microengines were immersed into solutions of aqueous H_2O_2 (2.5% v/v) as fuel and benzalkonium chloride (ADBAC) (0.5% v/v), as the surfactant, to determine the influence of white light on the mobility of the μ-engines. At lower concentrations of both chemicals, the generation of microbubbles is significantly reduced. Thus, the motility of the catalytic μ-engines is controlled by a small change in the fuel (H_2O_2 and/or surfactant) concentration.

These conditions allow us to investigate a concentration range close to the metastable state, that is, where the probability of stopping the μ-engines is high. Figure 1 A shows an optical microscopy image of a self-propelled μ-engine on a Pt-patterned silicon substrate (1 nm-thick Pt layer) placed in a Petri dish (≈53 mm in diameter) under the illumination of a tungsten lamp (inset in Figure 1 A). The speed of the μ-engines moving within the illuminated area is rapidly reduced and is zero after a few seconds (Figure 1 B). In Figure 1 B each point displays the position of the μ-engine after every 0.5 s (see the corresponding Video S1 in the Supporting Information). In a control experiment, we also study the motion of μ-engines above unpatterned silicon and glass substrates. Their speed does not decrease over time, despite an illumination of more than 1 min (see Figure S1 and Video S2 in the Supporting Information), indicating that the presence of a Pt substrate in proximity to the μ-engines affects the generation of microbubbles. To generate visible bubbles, the oxygen product from the catalytic breakdown of H_2O_2 needs to be accumulated within a μ-cavity. This is the case for our rolled-up microtubular engines, where the diffusion rates of the products are slower than on the planar substrates. It is important to note that we do not observe bubbles from the planar substrates when using the H_2O_2 fuel solution (i.e. 2.5% H_2O_2).

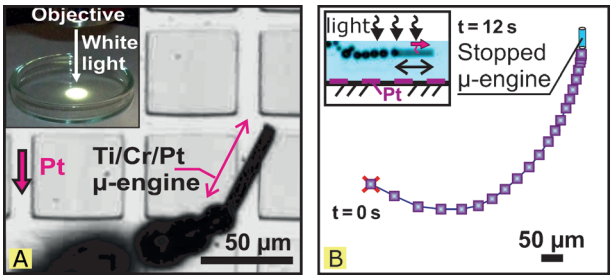

Figure 1. A) Optical image of a self-propelled Ti/Cr/Pt μ-engine moving above a platinum-patterned silicon surface. Inset: local illumination of the fuel solution containing the μ-engines. B) Tracked trajectory of a μ-engine stopped after 12 s of illumination above a Pt-patterned Si surface. The time interval between two spots in the plot is 0.5 s. Inset: optical image of the mobile μ-engines self-propelled above the patterned surface. See also Video S1 in Supporting Information.

[*] A. A. Solovev, Dr. E. J. Smith, Dr. C. C. Bof' Bufon, Dr. S. Sanchez, Prof. O. G. Schmidt
Institute for Integrative Nanosciences, IFW Dresden
Helmholzstr. 20, 01069 Dresden (Germany)
E-mail: s.sanchez@ifw-dresden.de

[**] This work was supported by the Volkswagen Foundation (grant number I/84 072). We thank R. Engelhardt, C. Krien, C. Vervacke, and R. Buckan for the help with the experiments. A. A. Solovev thanks Dr. G. Wang and Prof. Y. F. Mei for fruitful discussions.

Supporting information for this article is available on the WWW under http://dx.doi.org/10.1002/anie.201102096.

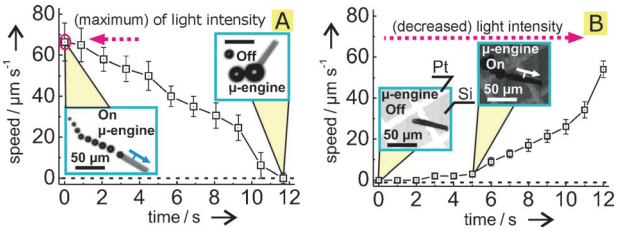

Figure 2. Switching the propulsion of individual μ-engines off (A) and on (B) using a white-light source. A) The μ-engines decelerate and stop after a 12 s exposure to the maximum power of the white-light source. The insets show moving (left inset) and stopped (right inset) μ-engines. B) Starting of the self-propulsion of a μ-engine by decreasing the intensity of light.

Figure 2 shows the analyzed deceleration of a μ-engine which was switched "off" (Figure 2 A and Video S1 in the Supporting Information, μ-engine #1) and switched on (Figure 2 B and Video S3 in the Supporting Information). Both studied μ-engines are propelled above a Pt-patterned silicon surface. First, the light intensity is turned to the maximum (Figure 2 A) which leads to a full stop of the μ-engine after a time-lapse of 12 s (from 65 to 0 $\mu m\,s^{-1}$). This phenomenon is also reversible, given that, by dimming the light source, a static μ-engine is activated and accelerates from 0 to 55 $\mu m\,s^{-1}$ as the light intensity is further decreased. In both studied cases, that is, start and stop, the phenomenon is not immediate and thus it requires a few seconds to either fully stop or to acquire maximum speed.

The speed of the μ-engines is directly related to the concentration of available hydrogen peroxide. Furthermore, the concentration of a surfactant in the fuel composition plays a significant role in the motion of the μ-engines because it reduces the surface tension inside the microtubes, allowing the fuel to wet the catalytic walls.[7,11] Thus, a small decrease in its concentration will also lead to a reduction of speed, as well as to the formation of larger bubbles. The degradation of surfactants within peroxide solutions by illumination with light has been well-studied for a photo-Fenton process[13] and photocatalysts.[14]

The insets in Figure 2 A show different bubble sizes before and after illumination of the fuel solution, which indicates that the surfactant and hydrogen peroxide concentration has been modified by exposure to light (see also the study on microbubbles at different peroxide and ADBAC concentrations at low intensity of white light in Figure S2 in the Supporting Information). In the case of the fast engines (inset showing a μ-engine switched on), the bubble expelled from the tube is almost equal in size to the diameter of the microtube. However, when the engine is off, larger bubbles are generated which is a clear indicator for a diminished surfactant concentration.[11]

By electrochemical measurements, we investigate the generation of oxidizing species from a H_2O_2 solution after illumination with white light. Figure S3 in the Supporting Information depicts the cyclic voltammetry measurements, showing an increase on the oxidation peak at 0.8 V (vs. Ag/AgCl) after illumination, indicating that oxygen is generated in the solution during illumination. Recently, it was demonstrated that the electrochemical oxidation of H_2O_2 into O_2 affects the speed of catalytic nanomotors.[15] H_2O_2 can decompose into O_2 which results in an increase in the anodic current when the solution is illuminated in the presence of a Pt catalyst. We performed control experiments to demonstrate that the generation of oxygen has no influence on the motion of the μ-engines. We continuously bubble oxygen into 1 mL of the fuel solution for 2 min. The analyzed data from twenty on-chip μ-engines shows that the frequency is not significantly altered (data not shown). In addition, Figure S2 A in the Supporting Information shows that reducing the concentration to less than 2 % H_2O_2 abruptly halts the engines, indicating that the oxidation of H_2O_2, rather than the generation of O_2 in the solution, is the key parameter.

Two effects in the system occur after illumination of the fuel solution in combination with thin Pt layers: 1) depletion of hydrogen peroxide fuel which results in a direct reduction of speed of the microjets and 2) decomposition of the surfactant molecules in close vicinity to the Pt surface. Both reasons are independently consistent, and both contribute to the full switching off of the engines.

Measurements of the surface tension confirm that the combination of light and Pt surfaces degrades the surfactant. This increases the surface tension of the solution (Note S4 in the Supporting Information) from 35 to 55 $mN\,m^{-1}$ after illuminating a 2 % H_2O_2 solution, containing a Pt patterned substrate, with a white-light source (Table S1 in the Supporting Information). In an additional experiment, we observe that for a fuel solution with a lower concentration of surfactant (i.e. higher surface tension), larger bubbles are released from the tubes (see Figure S2B in the Supporting Information).

We investigate the influence of light on μ-engines which are attached to a Pt-patterned Si substrate because the continuous motion of our self-propelled μ-engines makes a thorough study difficult. Figure 3 A shows the influence of the H_2O_2 concentration on the bubble generation at different light intensities and a constant ADBAC concentration (5 % v/v). A transition from 2 to 3 % v/v of H_2O_2 changed the initial bubble frequency from 1.5 to 7.25 Hz (light intensity 140 a.u.). This jump in frequency is 4.2 times higher relative to a jump in the peroxide concentration from 3 to 4 %. Despite the difference in the initial peroxide concentration, the bubble frequency decreases in all cases when the intensity of light reaches 190 a.u. Beyond this intensity, no more bubbles are released from the μ-tubes (yellow region on the plots). Figure 3 B shows data for μ-engines pumping in solutions of ADBAC concentrations ranging from 0.05–5 % v/v, whereas the concentration of hydrogen peroxide (4 % v/v) remains constant. Reducing the ADBAC concentration by one order of magnitude from 5 to 0.5 % does not produce an enormous change in the bubble frequency. However, decreasing it to 0.05 %, reduces the frequency to half of that of the initial frequency (from 8.2 Hz to 4.1 Hz). Consequently, it is clear that the release of bubbles is sensitive to both components of the fuel and to the intensity of light.

A reversible and rapid switching off or on is achieved with an increase or decrease in the white-light intensity (see Video S4 in the Supporting Information). This effect is local

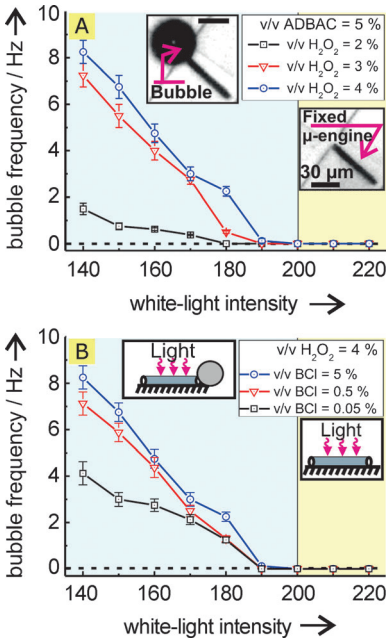

Figure 3. Bubble frequency of fixed μ-engines at different intensities of white light at varying A) H_2O_2 and B) ADBAC concentrations. The insets in Figure 3 B show the microbubble recoil from a μ-engine before (left) and after (right) being stopped by light. The error bars in both figures show statistical data of microbubble generation from individual μ-engines over a period of 4 s. The yellow region shows where the bubble frequency is zero and the blue region shows where the μ-engines are active.

and it takes place only within the illuminated region. For instance, if the illuminated area is moved along a surface containing fixed μ-engines, the regions that are no longer illuminated activate the μ-engines immediately, whereas the μ-engines located in illuminated regions are stopped (see Video S5 in the Supporting Information). We hypothesize that the reactivation of the μ-engines is due to a fast fluid diffusion from the nonilluminated surroundings (i.e. replenishment of nondegraded peroxide and surfactant, allowing for a recovery of the initial propelling conditions). Videos S4, S5, and S6 in the Supporting Information reveal the importance of distance between the Pt-patterned surface and the μ-engines in the required time to stop the engines. Microengines located at a certain distance above the Pt-substrate (from approximately 0.1 to 1.2 mm) need at least 10 s to be fully activated or stopped. On the contrary, the engines integrated on-chip start and stop within the first two seconds after exposure to light (the distance to the Pt-pattern is approximately 2 μm). This time delay strongly suggests that diffusion processes are taking place in the activation process of the μ-engines.

Given that white light is composed of all wavelengths ranging from blue (450 nm) to red (750 nm) light, a wavelength-dependent investigation of the system can be obtained by using a monochrometer. A supercontinuum white-light laser source in conjunction with a monochrometer is used to determine the wavelength and intensity influences of visible light on the frequency of the microbubbles. For this purpose, laser light, emitted from a fiber output of the monochromator, is irradiated on the sample surface. Figure S4 in the Supporting Information shows the experimental setup consisting of the laser, monochrometer, and a 50:50 beam splitter for in situ monitoring the predefined intensity of the irradiated light. The full width at half maximum of the wavelength of irradiated light (2 nm), is determined by the grating within the monochrometer and was measured separately with a fiber spectrometer. Figure 4 shows a quantitative analysis of the

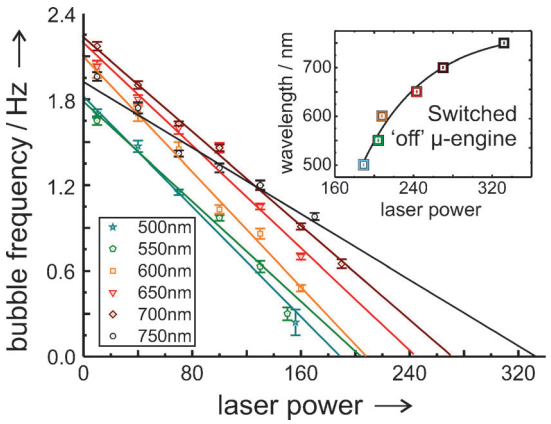

Figure 4. Dependence of the bubble frequency on the illuminating wavelength. The straight lines display linear fit functions to experimental data, extrapolated to zero where the μ-engines are no longer active. The inset shows a plot of the extrapolated points corresponding to the power required to switch off the μ-engines versus the laser wavelength. Below this curve, the μ-engines are switched off and no microbubbles are observed.

frequency of bubbles released from the μ-engines illuminated by laser light of different wavelengths and intensities (here 1 a.u. corresponds approximately to 1 μW) immersed in a 2 % v/v H_2O_2 and 0.5 % v/v ADBAC aqueous solution. The graph in Figure 4 shows experimental points and linear fit functions, showing the change in microbubble frequencies as a function of the laser power and wavelength, with step intervals of 50 nm (see Video S6 in the Supporting Information). The linear plots are extrapolated to a point of zero bubble frequency to determine the conditions required, that is, the light intensity and power, for stopping the μ-engines. The inset graph of Figure 4 shows a logarithmic fit to the extrapolated points. The region below the curve shows an area where a μ-engine is switched off and the region above the curve shows an area where a μ-engine is switched on. This data clearly indicates that the sensitivity of microbubble generation is highest at shorter wavelengths. Nevertheless, it is possible to fully stop the generation of microbubbles at longer wavelengths by increasing the intensity of light.

The energy of a photon depends on its wavelength (λ) and equals $E = hc/\lambda$, where c is the speed of light and h is the Planck constant. Subsequently, light with higher energy, corresponding to shorter wavelengths (i.e. for $\lambda = 500$ nm $E = 2.48$ eV, and $\lambda = 750$ nm $E = 1.65$ eV) degrades the H_2O_2 more rapidly. Error bars here were calculated as the standard deviation of 20 to 100 (depending on available data points) independent measurements of microbubble generation.

In conclusion, we demonstrated control over the propulsion of microbubble-driven Ti/Cr/Pt catalytic μ-engines using a light source which induces a local decrease of the hydrogen peroxide fuel and surfactant concentration. This process was mediated through illumination of the fuel solution above platinum-patterned silicon surfaces. Although white light can be used to switch off the propulsion of μ-engines, shorter wavelengths suppress the generation of microbubbles more rapidly relative to longer wavelengths. We believe that our results will open the door towards many practical applications including full wireless control over the propulsion of micro/nanomachines.

Experimental Section

Fabrication of rolled-up μ-engines: Catalytic tubular Ti/Cr/Pt μ-engines were prepared by rolled-up nanomembranes from sacrificial layers of a photoresist. Square patterns with a width of 50 μm were prepared on 1.5 inch silicon wafers. The photoresist ARP 3510 was spin-coated onto the silicon wafers at 3500 rpm for 35 s followed by a soft bake using a hotplate at 90 °C for 1 min and exposure to UV light with a Karl Suss MA56 Mask Aligner for 7 s. Patterns were developed in AR300 35:H_2O (1:1 v/v) solution. Using angular (75°) electron-beam deposition,[10] Ti/Cr (10/10 nm corresponding thickness) layers were deposited on the photoresist patterns, followed by magnetron sputtering of a 1 nm Pt layer. Microengines were rolled up by immersing the samples in acetone and dissolving the sacrificial photoresist layer. Samples were then rinsed with isopropanol and kept in a fluid to avoid the collapse of the μ-engines in air. Thereafter, they were immersed in the fuel solution containing hydrogen peroxide and ADBAC.

Preparation of the fuel solution: Solutions with different ADBAC (from 5×10^{-3} to 5 v/v %) and H_2O_2 (from 2 to 4 v/v %) concentrations were prepared. Aqueous solutions of hydrogen peroxide (30 v/v %, VLSI Technic, France) and benzalkonium chloride (ADBAC, Alfa Aesar GmbH, 50 v/v %) were freshly prepared before the experiments.

Light setup to control the μ-engines: An optical Zeiss Axio microscope was used for controlling the propulsion of the μ-engines by a white-light source. A tungsten lamp 12 V, 100W (Philips) was used for observing the motion of the μ-engines and controlling their motion by changing the intensity of the lamp. No additional light source was applied. The laser setup used to study the generation of microbubbles is described in the Supporting Information.

Recording videos and analysis: Videos were recorded using a high-speed video camera, Photonic Science, generating 50 frames per second. The camera is integrated into the Zeiss Axio Microscope and videos were analyzed with VirtualDub and ImageJ free imaging software.

The cyclic voltammograms were measured in a three-electrode electrochemical cell by using a μ-autolab typeIII potentiostat/galvanostat. Further details are given in the Supporting Information.

The surface tension was maesured by evaluating the drop profile at each concentration of surfactant in a computer-controlled KSV CAM101 optical contact angle and surface tension meter.

Received: March 24, 2011
Revised: September 5, 2011
Published online: September 20, 2011

Keywords: catalysis · electrochemistry · microengines · nanomachines · nanotechnology

[1] a) T. E. Mallouk, A. Sen, *Sci. Am.* **2009**, *300*, 72–77; b) T. Mirkovic, N. S. Zacharia, G. D. Scholes, G. A. Ozin, *ACS Nano* **2010**, *4*, 1782–1789; c) M. Pumera, *Nanoscale* **2010**, *2*, 1643–1649; d) A. Sen, M. Ibele, Y. Hong, D. Velegol, *Faraday Discuss.* **2009**, *143*, 15–27; e) J. Wang, K. M. Manesh, *Small* **2010**, *6*, 338–345; f) S. Sánchez, M. Pumera, *Chem. Asian J.* **2009**, *4*, 1402–1410; g) G. A. Ozin, I. Manners, S. Fournier-Bidoz, A. Arsenault, *Adv. Mater.* **2005**, *17*, 3011–3018.

[2] J. Wu, S. Balasubramanian, D. Kagan, K. M. Manesh, S. Campuzano, J. Wang, *Nat. Commun.* **2010**, *1*, 36.

[3] a) S. Sanchez, A. A. Solovev, S. Schulze, O. G. Schmidt, *Chem. Commun.* **2011**, *47*, 698–700; b) S. Balasubramanian, D. Kagan, C.-M. J. Hu, S. Campuzano, M. J. Lobo-Castanon, N. Lim, D. Y. Kang, M. Zimmerman, L. Zhang, J. Wang, *Angew. Chem.* **2011**, *123*, 4247–4250; *Angew. Chem. Int. Ed.* **2011**, *50*, 4161–4164.

[4] S. Sundararajan, P. E. Lammert, A. W. Zudans, V. H. Crespi, A. Sen, *Nano Lett.* **2008**, *8*, 1271–1276.

[5] K. M. Manesh, M. Cardona, R. Yuan, M. Clark, D. Kagan, S. Balasubramanian, J. Wang, *ACS Nano* **2010**, *4*, 1799–1804.

[6] J. Burdick, R. Laocharoensuk, P. M. Wheat, J. D. Posner, J. Wang, *J. Am. Chem. Soc.* **2008**, *130*, 8164–8165.

[7] A. A. Solovev, S Sanchez, M. Pumera, Y. F. Mei, O. G. Schmidt, *Adv. Funct. Mater.* **2010**, *20*, 2430–2435.

[8] a) M. Ibele, T. E. Mallouk, A. Sen, *Angew. Chem.* **2009**, *121*, 3358–3362; *Angew. Chem. Int. Ed.* **2009**, *48*, 3308–3312; b) Y. Hong, D. Velegol, N. Chaturvedi, A. Sen, *Phys. Chem. Chem. Phys.* **2010**, *12*, 1423–1435; c) T. R. Kline, A. Sen, *Langmuir* **2006**, *22*, 7124–7127.

[9] Y. Hong, M. Diaz, U. M. Córdova-Figueroa, A. Sen, *Adv. Funct. Mater.* **2010**, *20*, 1568–1576.

[10] Y. Mei, G. S. Huang, A. A. Solovev, E. Bermúdez Ureña, I. Mönch, F. Ding, T. Reindl, R. K. Y. Fu, P. K. Chu, O. G. Schmidt, *Adv. Mater.* **2008**, *20*, 4085–4090.

[11] A. A. Solovev, Y. F. Mei, E. Bermúdez Ureña, G. S. Huang, O. G. Schmidt, *Small* **2009**, *5*, 1688–1692.

[12] Y. F. Mei, A. A. Solovev, S. Sanchez, O. G. Schmidt, *Chem. Soc. Rev.* **2011**, *40*, 2109–2119.

[13] a) O. Horváth, R. Huszánk, *Photochem. Photobiol. Sci.* **2003**, *2*, 960–966; b) A. Cuzzola, M. Bernini, P. Salvadori, *Appl. Catal. B* **2002**, *36*, 231–237.

[14] a) J. Kou, Z. Li, Y. Yuan, H. Zhang, Y. Wang, Z. Zou, *Environ. Sci. Technol.* **2009**, *43*, 2919–2924; b) R. Abe, H. Takami, N. Murakami, B. Ohtani, *J. Am. Chem. Soc.* **2008**, *130*, 7780–7781.

[15] P. Calvo-Marzal, K. M. Manesh, D. Kagan, S. Balasubramanian, M. Cardona, G.-U. Fleichsig, J. Posner, J. Wang, *Chem. Commun.* **2009**, 4509–4511.

